Resonant effect of Zener tunneling current

M. Morifuji, T. Imai, and C. Hamaguchi
Department of Electronic Engineering, Osaka University, Suita, Osaka 565-0871, Japan

A. Di Carlo
INFM-Department, Electronic Engineerig, University of Rome "Tor Vergata," 00133 Roma, Italy

P. Vogl, G. Böhm, G. Tränkle, and G. Weimann
Walter Schottky Institute, Technical University of Munich, D-85748 Garching, Germany
(Received 17 January 2002; published 29 May 2002)

We report the observation of a resonant effect of the Zener current through a *p-i-n* diode structure. The second derivative of the *I-V* characteristics, measured with a lock-in technique, shows several pronounced peaks. These peaks indicate that quasilocalized states in a quantum well in the intrinsic region are in resonance with Zener current. A calculation of the tunneling current based on tight-binding theory shows good agreement with our experimental results. The same holds for the calculated energetic positions of the localized electronic states. Altogether, these results indicate that the Zener current gets modulated due to Wannier-Stark resonances.

DOI: 10.1103/PhysRevB.65.233308 PACS number(s): 73.40.Gk, 73.63.Hs

In this paper, we report the observation of Wannier-Stark resonances in the electric current through a *p-i-n* diode. Wannier-Stark resonances have been well studied and observed by optical techniques,[1,2] but only a few preliminary dc current experiments have been reported that reveal this effect.[3–5] In the present case, the current is caused by Zener tunneling from the *p* region into the high-field intrinsic region and out again into the *n* region and becomes resonant through the buildup of Wannier-Stark resonances within the intrinsic region of the *p-i-n* diode.

Zener tunneling has attracted much attention since the early days of semiconductor science. It consists of an interband tunneling of carriers through the forbidden energy gap between the energy bands, and normally leads to a smooth increase of the current as a function of reverse bias until breakdown occurs. Resonant Zener tunneling, however, is an unusual phenomenon that has been predicted in Ref. 6 to occur in *p-i-n* diodes but has proven to be extremely difficult to observe. Recently, a modulated Zener current due to localized carriers has been observed in multiquantum well structures but the origin of the modulation has not been analyzed in detail yet.[7–9]

In principle, the resonant Zener tunneling effect resembles the well-known resonant tunneling effect in multiquantum wells which is very well understood. However, the combination of field-dependent barriers, multiband effects, and high spatially inhomogeneous electric-field effects has hampered the study of electrically driven and ballistic Wannier-Stark-induced resonant tunneling phenomena so far.

The complex valence-band structure and the different effective masses of valence and conduction bands render the conventional effective-mass approximation less useful for a detailed theoretical understanding of the Zener tunneling. The most common theoretical approach for the Zener tunneling current[10] has been a combination of $\mathbf{k}\cdot\mathbf{p}$ perturbation theory and the WKB method, but assumes homogeneous electric fields, which is not suitable for the present *p-i-n* diode. A more general and realistic approach for calculating the electric current through tunneling structures is based on the empirical tight-binding theory,[6,11–13] which allows one to properly take into account many electronic bands as well as spatially inhomogeneous electric fields. This theory has enabled one to calculate the Zener current through any type of heterostructures,[6,14,15] and predict the resonant Zener current.

The physical mechanism giving rise to the resonant Zener current can be illustrated by a schematic band diagram of a *p-i-n* diode as shown in Fig. 1. In the intrinsic region of the *p-i-n* diode, there are two barriers that enhance the confinement of carriers in the central area. By applying a sufficiently high reverse voltage, the valence band in the *p* region and the conduction band in the *n* region start to overlap in energy, so that a ballistic current can flow through the forbidden gap. This is the Zener tunneling current that normally increases monotonously with the reverse voltage. In the present case, however, the formation of quasilocalized electric-field-dependent states in the quantum well can lead to resonances in the Zener current. Once a quasilocalized state becomes resonant, it will contribute to the current also for higher volt-

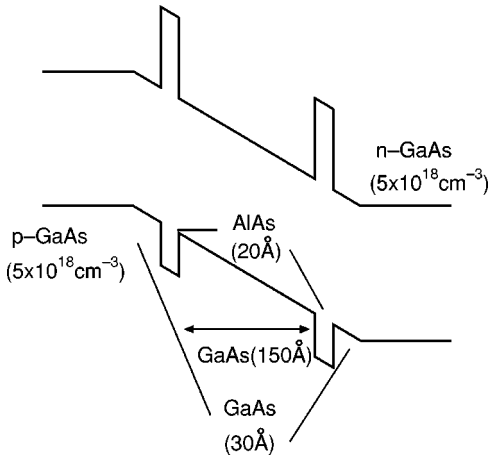

FIG. 1. Schematic band diagram of the sample used in this study.

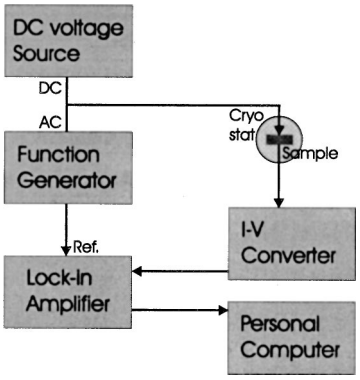

FIG. 2. Schematic setup for measurements of derivative of current-voltage characteristics.

ages so that we may expect a steplike increase of the Zener tunneling current with reverse bias.

The sample structure used in this study is shown in Fig. 1. A quantum well of AlAs(20 Å)–GaAs(150 Å)–AlAs(20 Å) is set into the intrinsic region of a *p-i-n* diode of GaAs. The doping concentration is 5.0×10^{18} cm^{-3} for both the *p* and the *n* regions. Between the quantum wells and the doped regions, 30-Å nondoped GaAs spacer layers have been inserted so as to prevent the diffusion of dopant ions into the quantum well.

In order to measure the tunneling current, the sample wafer has been etched into a mesa structure with 20×20 μm^2 sized mesas. Since the signal due to current resonances is expected to be very weak, we have measured the derivative of tunneling current by using a lock-in technique. A schematic graph of the setup is depicted in Fig. 2. We have applied a dc reverse bias to the sample that has been set into a cryostat. In addition, a small amplitude ac voltage has been applied from a function generator. We can write the current I as

$$\begin{aligned} I &= I[V_{\rm dc}+V_{\rm ac}\cos(\omega t)] \\ &\simeq I(V_{\rm dc})+\frac{dI}{dV}V_{\rm ac}\cos(\omega t)+\frac{1}{2}\frac{d^2I}{dV^2}[V_{\rm ac}\cos(\omega t)]^2+\cdots \\ &= I(V_{\rm dc})+\frac{dI}{dV}V_{\rm ac}\cos(\omega t)+\frac{V_{\rm ac}^2}{4}\frac{d^2I}{dV^2}\cos(2\omega t)+\cdots, \quad (1) \end{aligned}$$

where $V_{\rm dc}$ is the dc voltage and $V_{\rm ac}$ is the amplitude of the ac voltage with frequency ω. This equation indicates that one can measure the first derivative of the current by picking up the ω component of the current. In a similar way, the second derivative can be obtained from the 2ω component, employing a lock-in amplifier. We have chosen 60 mV and 80 mV for the amplitude of the ac voltage for the first and second derivative measurements, respectively. The frequency of the ac voltage has been set to 1100 Hz and all measurements have been carried out at 4.2 K.

The results of our measurements are depicted in Fig. 3. The solid curve shows the measured current-voltage characteristics, whereas the dotted and the dashed curves represent the first and the second derivative characteristics, respectively, which have been obtained by using the lock-in technique described above. The latter two curves are plotted in arbitrary units with some relative offset. We note that there is a tradeoff in setting the values for the ac voltage as given above. A high value of $V_{\rm ac}$ enhances the signal, but simultaneously enhances the neglected higher order terms in Eq. (1), which also contribute to the ω and 2ω components of the current. Thus, we have reduced the ac voltage amplitude $V_{\rm ac}$ as much as possible. Still, it is difficult to evaluate the absolute values of the derivative signals, and we have not attempted to do so.

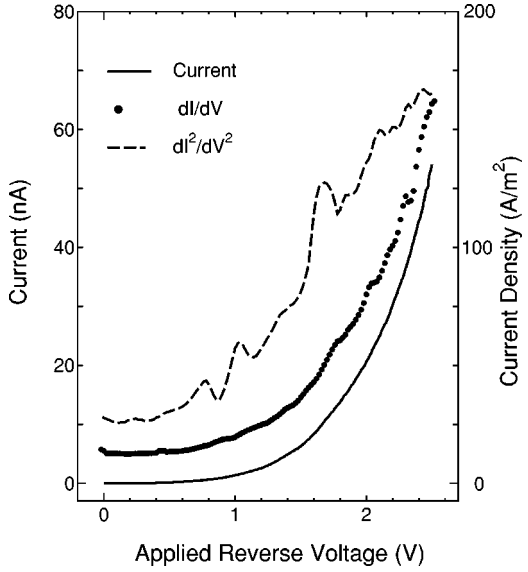

FIG. 3. Measured current-voltage characteristics are shown by solid curve. The first and the second derivative are shown by dotted and dashed curves, respectively.

The second derivative curve exhibits clear peaks in the voltage region between 0.8 and 2.4 V. While the structures in the first derivative curve are much weaker, the peak positions of both curves are consistent with one another. This is shown in Fig. 4, where we compare the data obtained by numerical differentiation of the first derivative curve with the measured second derivative of the current. While the reliability of structures in a merely numerically calculated derivative of noisy data is always debatable, it is the good one-to-one correspondence between the peak positions of both curves in the present case that indicates these current maxima to constitute physically significant resonances indeed.

In order to analyze these signals in detail, we have calculated the Zener tunneling current by using the sp^3s^* empirical tight-binding theory[16] with the parameters given in Ref. 6. The Zener current density as a function of the applied reverse voltage V is given by

$$\begin{aligned} j(V) = \frac{-e}{(2\pi)^3\hbar}\sum_{n,n'}\int d\mathbf{k}_\parallel \int dE T_{(n\mathbf{k}\to n'\mathbf{k}')}(E,V) \\ \times[f_{\rm p}(E_{n\mathbf{k}})-f_{\rm n}(E_{n'\mathbf{k}'}-eV+V_D)], \quad (2) \end{aligned}$$

where $E_{n\mathbf{k}}$ is the electronic energy for band n and wave vector $\mathbf{k}$ in the (field-free) asymptotic n and p regions,

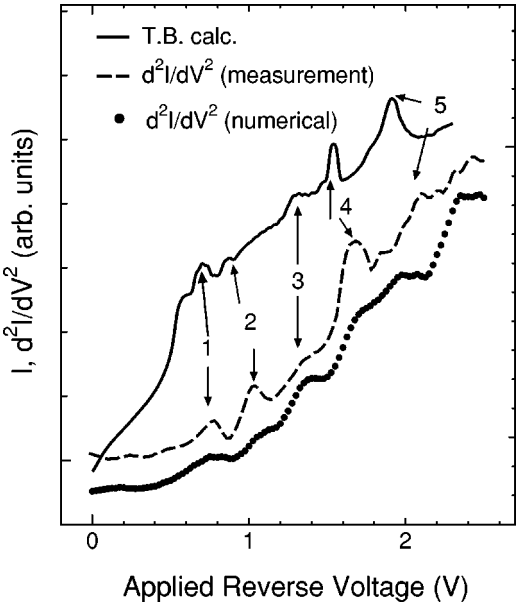

FIG. 4. The solid curve shows Zener tunneling current calculated from tight-binding theory. The dashed curve is the measured second derivative of current which is already shown in Fig. 3. The dot is second derivative numerically obtained from measured first derivative curve.

$f_c(E_{n\mathbf{k}})$ $(c=n,p)$ are the Fermi distribution function in these regions, and V_D is the built-in voltage drop at the contacts due to the p-n junction. $T_{(n\mathbf{k}\to n'\mathbf{k}')}(E,V)$ is the tunneling probability from the valence-band states in the p region to the conduction-band states in the n region. It can be written as

$$T_{(n\mathbf{k}\to n'\mathbf{k}')}(E,V)=\left|\frac{f_{n'\mathbf{k}'}}{f_{n\mathbf{k}}}\right|^2\frac{v_{n'\mathbf{k}'}}{v_{n\mathbf{k}}}, \tag{3}$$

where $f_{n\mathbf{k}}$ and $f_{n'\mathbf{k}'}$ are the amplitudes of the initial and final states $|n\mathbf{k}\rangle$ and $|n'\mathbf{k}'\rangle$, respectively, and the electron velocities of these states are denoted by $v_{n\mathbf{k}}$ and $v_{n'\mathbf{k}'}$, respectively. These amplitudes of the electronic states can be obtained from the transfer-matrix equation

$$\begin{bmatrix} f^+_{n'\mathbf{k}'} \\ f^-_{n'\mathbf{k}'} \end{bmatrix}=\begin{bmatrix} M_{++} & M_{+-} \\ M_{-+} & M_{--} \end{bmatrix}\begin{bmatrix} f^+_{n\mathbf{k}} \\ f^-_{n\mathbf{k}} \end{bmatrix} \tag{4}$$

with the scattering boundary condition $f^+_{n\mathbf{k}}=1$ and $f^-_{n'\mathbf{k}'}=0$. Here, the superscripts $\pm$ indicate the direction of the electronic motion. We note that our notation actually corresponds to a single-band case, which we give here for the sake of clarity but the full multiband expression[6,11–13] has been used in the calculations. In Eq. (4), the transfer-matrix M is given by

$$M=S_p^{\dagger}\prod_j T_j(\mathbf{k}_{\|},E-V_j)S_n, \tag{5}$$

where S_p and S_n are the eigenvector matrices corresponding to the electron states in the p and n region, respectively. T_j is a matrix that connects the scattering amplitude at the jth atomic layer with its adjacent layer, and V_j is voltage in the jth atomic layer. This matrix T_j can be written in terms of the tight-binding couplings between adjacent atomic orbitals. Therefore, one can calculate $|f_{n'\mathbf{k}'}/f_{n\mathbf{k}}|^2$ from Eqs. (4) and (5) by connecting the amplitudes layer by layer. In order to avoid numerical instabilities, we have used the method developed in Ref. 12.

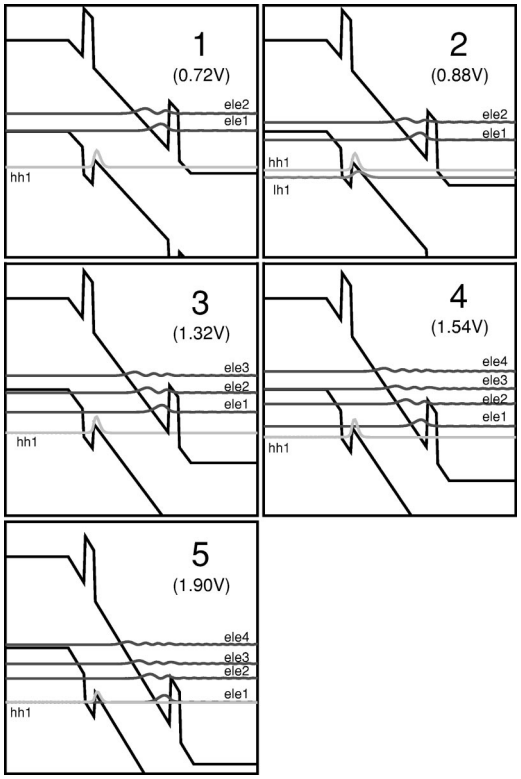

FIG. 5. Band-edge profile and charge densities in the quantum well calculated based on the effective mass approximation.

In Fig. 4, the solid curve shows the I–V characteristics as calculated from Eqs. (2)–(5). We have not carried out the full in-planar $\mathbf{k}_{\|}$ integration but evaluated the integrand only at $\mathbf{k}_{\|}=(0,0)$. This approximation is reasonably well justified in the present tunneling current calculation, since the larger $\mathbf{k}_{\|}$ terms are exponentially suppressed in the tunneling process due to the quadratically increasing band gap. Furthermore, we note that the current in Fig. 3 has been plotted on a logarithmic scale, whereas the derivative curves are not. This is inadequate for a quantitative comparison between experiment and theory, which is beyond the scope of this paper. However, the plots in Figs. 3 and 4 clearly show the good correspondence between the calculated and measured peak positions. This kind of agreement indicates that the peaks in the measured derivative characteristics are indeed due to the resonant Zener tunneling current.

In order to further confirm the physical origin of the observed resonances, we have calculated the electronic energies and wave functions by using a simple effective-mass approximation. Although it is possible to calculate the wave functions directly from the tight-binding theory, their envelopes reflect their character and shape more transparently than the complete atomic wave functions and suffice for the

present comparison. Figure 5 shows the calculated band-edge profiles for applied reverse voltages of 0.72, 0.88, 1.32, 1.54, and 1.90 V, respectively. These voltages correspond to those where the measured second derivatives of Zener current exhibits maxima. In addition to the band edges, Fig. 5 depicts the charge densities of the low-lying quasibound states. In the first diagram (labeled by 0.72 V), we see that the first resonant state (labeled ele1) is aligned with the top of the valence band in the *p* region. This corresponds precisely to a resonance condition, where the localized Wannier-Stark state resonantly enhances the tunneling probability from the valence-band edge of the *p* region and into the conduction band of the *n* region. Similarly, at the voltages of 1.32, 1.54, and 1.90 V, the higher-lying electronic states ele2, ele3, and ele4 become aligned with the top of the valence band, respectively, which fits very nicely to the observed peak positions in the current derivatives. This clear correspondence allows us to ascribe the measured peaks to the resonant Zener tunneling effect due to localized Wannier-Stark electronic states in the intrinsic region.

As one may expect from a simple effective-mass approximation, not all of the observed peaks can be uniquely attributed to some resonance. In the diagram labeled by 0.88 V, for example, the valence-band edge is not in resonance with some of the localized states. The current peak at 0.88 V may be due to a light-hole state (labeled lh1), although the alignment is not perfect in the effective-mass calculation.

The states ele3 and ele4 are actually seen to be semiconfined states at the voltage shown in Fig. 5. Their extended character enhances the resonant effect, which explains why the calculated peaks labeled 4 and 5 in Fig. 4 are more pronounced than the other ones. In the measured signals, however, we cannot clearly identify this effect. This may be due to nonresonant current contributions, which certainly tend to get stronger with larger reverse bias.

There are a few studies that have observed modulation in Zener current due to embedded two quantum wells.[7–9] In these studies, however, the modulation is attributed to the resonance between electron and hole in the adjacent wells. On the other hand, the present data are from the sample with a single quantum well, and clearly indicate the interaction between ballistic Zener tunneling electrons and the quasilocalized state in the quantum well.

In conclusion, we have measured the resonant Zener tunneling current through a *p-i-n* diode with a quantum well in its intrinsic region that forms localized Wannier-Stark resonances. In addition to current, we have measured the first and second derivatives of the current. We find these derivative characteristics to show several pronounced peaks that show good correspondence with the calculated Zener current and the energetic positions of the localized electronic states within the intrinsic region. These results clearly indicate that we have been able to observe the resonant states all electrically in the Zener current.

[1] F. Agulló-Rueda, E. E. Mendez, and J. M. Hong, Phys. Rev. B **40**, 1357 (1989).
[2] E. E. Mendez, F. Agulló-Rueda, and J. M. Hong, Appl. Phys. Lett. **56**, 2545 (1990).
[3] M. Morifuji, K. Murayama, C. Hamaguchi, A. Di Carlo, P. Vogl, G. Böhm, and M. Sexl, Phys. Status Solidi B **204**, 368 (1997).
[4] C. Hamaguchi, M. Yamaguchi, H. Nagasawa, M. Morifuji, A. Di Carlo, P. Vogl, G. Böm, G. Trankle, and G. Weimann, Jpn. J. Appl. Phys., Part 1 **34**, 4519 (1995).
[5] L. Bürkle, F. Fuchs, E. Ahlswede, W. Pletschen, and J. Schmitz, Phys. Rev. B **64**, 045315 (2001).
[6] A. Di Carlo, P. Vogl, and W. Pötz, Phys. Rev. B **50**, 8358 (1994).
[7] J. Allam, F. Beltram, F. Capasso, and A. Y. Cho, Appl. Phys. Lett. **51**, 575 (1987).
[8] R. A. G. Cinelli, V. Piazza, S. de Franceschi, M. Lazzarino, and F. Beltram, Appl. Phys. Lett. **73**, 3553 (1998).
[9] N. El-Zein, M. Deshpande, G. Kramer, J. Lewis, V. Nair, M. Kyler, S. Allen, and H. Goronkin, *Proceedings of International Conference on Indium Phosphide and Related Materials* (IEEE, Williamsburg, 2000), p. 146.
[10] E. O. Kane, J. Appl. Phys. **32**, 83 (1961).
[11] J. N. Schulman and Y.-C. Chang, Phys. Rev. B **27**, 2346 (1983).
[12] J. N. Schulman and D. Z.-Y. Ting, Phys. Rev. B **45**, 6282 (1992).
[13] Y.-C. Chang and J. N. Schulman, Phys. Rev. B **25**, 3975 (1982).
[14] M. Morifuji and C. Hamaguchi, Phys. Rev. B **52**, 14 131 (1995).
[15] M. Morifuji, K. Taniguchi, and C. Hamaguchi, Surf. Sci. **361/362**, 201 (1996).
[16] P. Vogl, H. P. Hjalmarson, and J. D. Dow, J. Phys. Chem. Solids **44**, 365 (1983).